PERGAMON

International Journal of Solids and Structures 38 (2001) 3927–3944

INTERNATIONAL JOURNAL OF SOLIDS and STRUCTURES

www.elsevier.com/locate/ijsolstr

A cohesive zone model for fatigue crack growth in quasibrittle materials

B. Yang [a], S. Mall [b,*], K. Ravi-Chandar [c]

[a] *Department of Aeronautics and Astronautics, Air Force Institute of Technology, Wright-Patterson AFB, Building 640, 2950 p. St., OH 45433-7765, USA*

[b] *Materials and Manufacturing Directorate, (AFRL/MLLN), Air Force Research Laboratory, Air Force Institute of Technology, Wright-Patterson AFB, Building 640, 2950 p. St., OH 45433-7765, USA*

[c] *Department of Mechanical Engineering, University of Houston, Houston, TX 77204, USA*

Received 13 October 1999

Abstract

A cohesive zone model for fatigue crack initiation and growth in quasibrittle materials is proposed in the present paper. While bulk material is modeled to be linearly elastic, the softening material in the cohesive zone and cracks are modeled to be internal singular surfaces in the elastic body. The interactions of the singular surfaces are described in a cohesive force law and a Coulomb-type friction law if in contact. The cohesive zone material is modeled to accumulate damage not only along the damage locus but also along an unloading path underneath it, enabling a simulation of fatigue damage and crack growth without the ad hoc imposition of a law of growth rate within the cohesive zone model. The maximum principal stress criterion is used to advance a tip of the cohesive zone in the direction of the maximum principal stress when it reaches the critical value of material strength. The physical crack tip is grown as a natural process of debonding of the cohesive zone under cyclic loading, which, in contrast, may be subcritical with energy dissipation less than the material toughness under static loading. The boundary value problem formulated for fatigue crack growth incorporating the cohesive zone model is nonlinear due to the history dependence of the cohesive zone, and is solved efficiently using the iterative single-domain dual-boundary-element method of successive over-relaxation. It is demonstrated through examples that the present model is capable of predicting fatigue crack initiation as well as growth in a unified way. It is also shown that the cohesive zone model is more advantageous and flexible in handling fatigue cracks under arbitrary loading than the classical singularity-based fracture mechanics approach. Published by Elsevier Science Ltd.

Keywords: Fatigue crack initiation modeling; Fatigue crack growth modeling; Cohesive zone model; Progressive damage; Quasibrittle materials; Boundary element method

* Corresponding author. Tel.: +1-937-255-3069; fax: +1-937-656-7621.
E-mail address: shankar.mall@afit.af.mil (S. Mall).

0020-7683/01/$ - see front matter Published by Elsevier Science Ltd.
PII: S0020-7683(00)00253-5

1. Introduction

It is natural that under progressive loading, a material softens, forming a narrow band of localized deformation, such as an adiabatic shear band in metals, or a craze in glassy polymers. Subsequent deformation may lead to creation of new surfaces, i.e., fracture at the location. The localized, damaged material may be modeled to be a pair of surfaces with no volume between and its action replaced by an equivalent traction on the surfaces. Following Dugdale (1960) and Barenblatt (1962), this idea has been applied extensively to materials which are commonly classified as quasibrittle materials such as glassy polymers, rocks, reinforced ceramics, concrete, composites, etc. The resulting models are variously called the cohesive crack model, the strip yield model, the cohesive layer model, the fictitious crack model, the bridged zone model, and the cohesive zone model, with only slight differences in the formulation (see Yang and Ravi-Chandar (1998a) for a classification of these models). In particular, using the fictitious crack model (Hillerberg et al., 1976), a number of researchers have widely studied size effects (Bazant et al., 1994), ductile–brittle transition (Carpinteri, 1994), and snap-back instability (Carpinteri, 1994; Bazant and Li, 1995) in concrete. A rate-dependent cohesive force law was considered in application to concrete-like materials (Bazant and Li, 1997) and ceramic matrix composites (Begley et al., 1997). In these previous investigations, the crack path was prescribed to be along a line of symmetry of the loading configuration. Xu and Needleman (1994) and Ortiz (1996) incorporated a cohesive traction between elements in the finite element formulation to study dynamic crack branching and fragmentation under arbitrary loading. However, in their model, the freedom for a crack to select paths between elements is limited due to finite number of elements in a practical numerical simulation. Yang and Ravi-Chandar (1998b) introduced the iterative single-domain dual-boundary-element formulation incorporating the cohesive zone model for elastostatic cracks in which a crack may be grown along an arbitrary path governed by the imposed failure criterion.

In these models (hereafter referred to as the cohesive zone model, for simplicity), a softening traction–displacement jump relationship with finite strength is used to characterize the interaction of the cohesive surfaces. When incorporating it in a crack formulation, the problem is well posed, and the singularity appearing in conventional fracture mechanics can be eliminated partially as in the case of a bridged zone model or completely as in others. In the latter case with the singularity completely removed, the energy balance law is satisfied automatically instead of being a "condition" as in the singularity-based fracture mechanics approach. Crack growth can be readily simulated as a consequence of continuous debonding of the cohesive zone material without a fracture criterion a priori. However, a law for the induction of bulk material into the cohesive zone, i.e., propagation of the cohesive zone tip, is needed to complete the formulation of crack growth. The softening constitutive law of the cohesive zone material is obviously the key component in the cohesive zone model, determining completely the debonding behavior under various loading conditions. In the original cohesive zone modeling, Dugdale (1960) assumed a constant variation of traction along the plastic strip zone and Barenblatt (1962) used a typical cohesive law for the atomic debonding. In subsequent investigations, a linear or bilinear relationship of traction and crack opening displacement has been commonly used. It was suggested that a bilinear relationship works well to simulate the global behavior of a cracking material such as concrete and ceramic. However, the behavior of the cohesive zone material was confined to the damage locus, and a study of crack development was limited to cases under monotonic loading and without complicated crack interaction. Recently, Yang and Ravi-Chandar (1996, 1998a,b) have considered the softening cohesive law with unloading effects, enabling a simulation of partial development of the cohesive zone at structural instability, complicated crack interaction, dynamic crack arrest, etc. Ortiz (1996) and Li et al. (1998) have also considered similar local unloading effects in their models of dynamic fragmentation and crack interaction. In all these works, the unloading and the subsequent reloading were assumed to follow the same path until reaching the damage locus. The linear process of unloading and reloading is incapable of modeling the subcritical crack growth

under cyclic loading; the fracture process zone (the cohesive zone) eventually stabilizes with no further damage under cyclic loading, as shown by Yang and Ravi-Chandar (1998a). On the other hand, de-Andres et al. (1999) extended the cohesive zone model with the linear unloading–reloading law to the finite element analysis of the fatigue crack growth observed experimentally in a shaft; in their formulation, the damage parameter of the cohesive zone material was explicitly adjusted with increasing number of loading cycles. In other words, the dependence of the damage process on the cyclic loading was not intrinsically included in the cohesive force law, which results in the lack of predictability of the fatigue life by the model. In the present work, we model fatigue crack growth in quasibrittle materials within the cohesive zone model, with a revised cohesive force law taking into account the differences between unloading and reloading paths at all stages of the cohesive zone. Irreversible damage in the cohesive zone material is assumed to accumulate not only along the damage locus but also during an unloading path underneath it. This idea can be motivated by observation of degradation of cohesive zone under cycling loading conditions. By this model, the subcritical crack growth due to cyclic loading can be predicted. Therefore, the fatigue behavior of a material may be studied under arbitrary loading conditions provided that the property of the cohesive zone is given. The problem is then reduced to finding such a cohesive force law for a specific material either by experiment or by a micromechanical model.

The present paper is organized in the following way. In Section 2, we describe the cohesive zone model for fatigue crack growth in a linearly elastic body with the cohesive zone material and cracks modeled as internal singular surfaces. A law in a general polynomial form for the interaction of the singular surfaces, which takes account of cumulative damage under cyclic loading, is proposed. The maximum principal stress (MPS) criterion is used for induction of bulk material into the cohesive zone. The crack contact and friction effects are also considered by using a Coulomb-type friction law, allowing a simulation of fatigue crack growth under arbitrary loading conditions. In Section 3, a number of simulations of the fatigue crack growth under pure mode I and mixed-mode loading conditions are presented and discussed in detail. The problem is solved efficiently by using the iterative single-domain dual-boundary-element method of successive over-relaxation (Yang and Ravi-Chandar, 1998b). The predicted fatigue behaviors of the material are interpreted in terms of conventional fatigue parameters. The capability of this model is demonstrated by these examples. Some conclusions are drawn in Section 4.

2. A cohesive zone model for fatigue crack growth in quasibrittle materials

2.1. Linearly elastic solids with singular surfaces

We consider a homogeneous, isotropic, linear elastic body Ω with external surfaces Γ^{ex} and internal singular surfaces Γ^{c}, as shown in Fig. 1. These surfaces $\Gamma^{\mathrm{ex+c}}(=\Gamma^{\mathrm{ex}}\cup\Gamma^{\mathrm{c}})$ are assumed to be smooth piecewise. The equilibrium equations at a point $x\in\Omega$ are

$$\sigma_{ij,j}+b_i=0, \tag{1}$$

where σ_{ij} are the components of the stress tensor, b_i are the components of the body force per unit volume, and j indicates partial differentiation with respect to x_j. The indices i and j range from 1 to 3 for three-dimensional problems and from 1 to 2 for two-dimensional problems, and refer to Cartesian coordinate directions. When an index in a subscript is repeated in any particular term, a summation over that index is implied. Note that, however, the convention of summation due to Einstein is not applied to superscript indices. The stress–displacement relationships are

$$\sigma_{ij}=\lambda\delta_{ij}u_{k,k}+\mu\left(u_{i,j}+u_{j,i}\right), \tag{2}$$

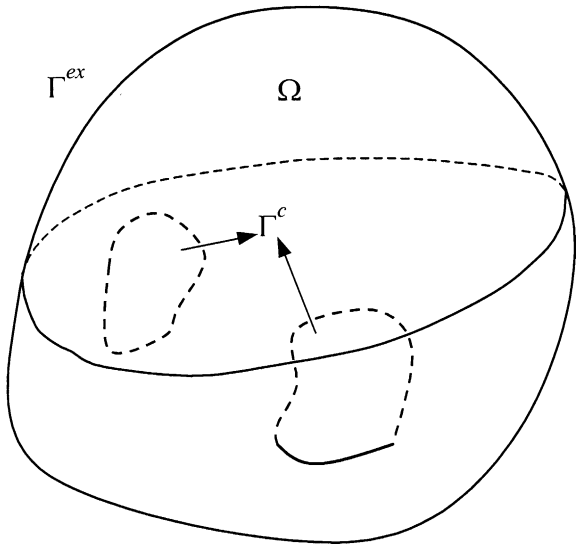

Fig. 1. A homogenous, isotropic, linearly elastic body Ω with smooth external boundary Γ^{ex} and singular surfaces Γ^{c} in equilibrium.

where λ and μ (shear modulus) are the Lame constants, u_i are the components of the displacement vector, and δ_{ij} is the Kronecker delta which is equal to 1 if $i = j$, and 0 otherwise. The Lame constants are related to Young's modulus E and Poisson's ratio v by $\mu = E/2(1 + v)$ and $\lambda = vE/(1 + v)(1 - 2v)$. By substituting Eq. (2) into Eq. (1), Navier's equations are obtained:

$$(\lambda + \mu)u_{k,ki} + \mu u_{i,kk} + b_i = 0. \tag{3}$$

In order to ensure unique solutions to Eq. (3), appropriate boundary conditions along Γ^{ex} and Γ^{c} need to be imposed, as addressed below.

Consider first the appropriate boundary condition for the external boundary Γ^{ex}. If either the displacement u_i or the traction $p_i(= \sigma_{ij}n_j)$ in each coordinate is given for a boundary point $\boldsymbol{x} \in \Gamma^{ex}$,

$$u_i = \overline{u}_i \qquad \text{or} \qquad p_i = \overline{p}_i \text{ on } \Gamma^{ex}, \tag{4}$$

the problem is well posed. The bar on the top of the symbols indicates a prescribed function. In the definition of traction, n_j is outward normal vector at the boundary point to the surface. If the given boundary condition is not so simple as, for example, at a boundary point fixed to a foundation through a nonlinear spring, some care must be taken in the formulation of the boundary value problem and in the procedure to solve it. Consider then the appropriate boundary condition for the singular surfaces Γ^{c}. The traction p_i on Γ^{c} and the displacement jump w_i across the singular surface Γ^{c} are assumed to be correlated by the following equation,

$$p_i = k_{ij}\left(w_j - w_j^{(0)}\right) \text{ on } \Gamma^{c} \text{ with } w_i = u_i^{-} - u_i^{+}, \tag{5}$$

where k_{ij} are the components of the stiffness tensor for the singular surfaces which may be a function of p_i, w_i, $\dot{w}_i$ and a number of other internal parameters, $w_i^{(0)}$ are the components of the residual displacement jump which may also be a function of the internal parameters, and u_i^{+} and u_i^{-} are the displacements on either side of the singular surfaces Γ^{c+} and Γ^{c-}. The dot on the top of w_i represents time derivative of the quantity.

The singular surfaces may be either opening or in contact. In the first case, if k_{ij} are identical to zero, the singular surfaces are consequently traction-free cracks, and the resulting stress field around the crack tip is singular (Williams, 1957). If k_{ij} are not trivial, the singular surfaces represent the localized, softening part of a material, leading to *the cohesive zone model of a crack*. A function describing the evolution of k_{ij} with crack opening is called the cohesive force law. With the nontrivial traction, the singular stress field at the crack tip can be eliminated. In the contact mode, Eq. (5) is appropriate only for description of the tangential interaction of the singular surfaces. The constraint condition of zero normal displacement jump,

$$w_i n_i = 0, \tag{6}$$

is needed to complete the formulation. In addition, the tangential traction may also be coupled to the normal pressure due to the frictional effect, described for example by a Coulomb-type friction law.

2.2. A cohesive force law for fatigue crack growth

The key component in the cohesive zone model is the cohesive force law, which determines the response of a crack under various loading conditions. In the vast literature on cohesive zone models, unloading effects in the cohesive zone have seldom been considered, except by a few groups (Ortiz, 1996; Yang and Ravi-Chandar, 1996, 1998a,b; Li et al., 1998). However, in their formulations, the loading and unloading paths were assumed to be linear and identical, resulting in no accumulation of damage under cyclic loading. de-Andres et al. (1999) attempted to apply the same cohesive force law associated with a law for decay of stiffness with loading cycles to study the fatigue crack growth observed experimentally in a shaft. Since the law for decay of stiffness was given with respect to the loading cycles only, the resulting formulation is unable to make a prediction of fatigue under arbitrary loading. In this section, we describe a law for the cohesive zone, which is appropriate for prediction of fatigue crack growth, and discuss the experimental characterization of such a law.

For a class of materials such as glassy polymers and soft-fiber reinforced composites, the behavior of the cohesive zone may be modeled by using the line spring model as shown in Fig. 2a (see Yang and Ravi-Chandar, 1998b for details). In the following, this line spring model is adopted because it significantly

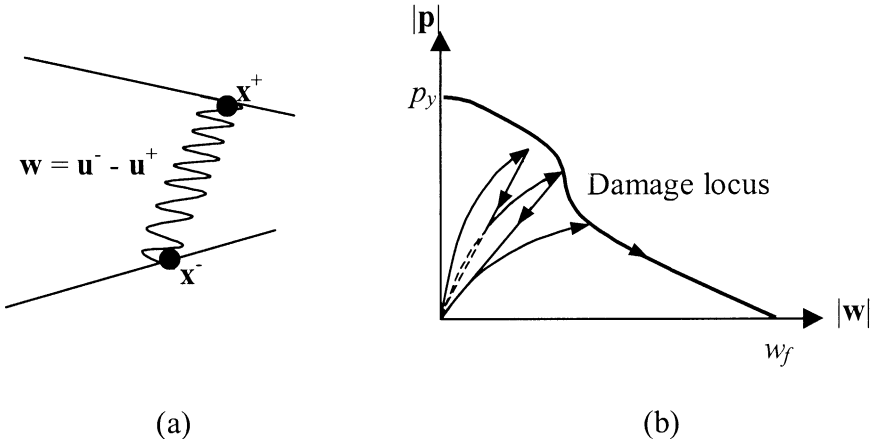

Fig. 2. (a) Illustration of two originally coincident points of a cohesive zone in the opening mode connected by the line spring and (b) schematic diagram of the constitutive law of the line spring in terms of the magnitudes of the traction and displacement jump vectors. The arrows indicate a deformation path. If the cohesive zone is in contact mode, the two points, x^+ and x^-, are separated only in the tangential direction, with $w_i n_i = 0$, and the frictional force may be activated. Note that it is assumed that the residual displacement jump $w_i^{(0)} = 0$.

simplifies the description and discussion by reducing the stiffness tensor k_{ij} to a scalar k (for opening mode of the cohesive zone). Furthermore, only the case in two dimensions with trivial residual displacement jump ($w_i^{(0)} = 0$) is considered. Under these conditions, the cohesive force law, Eq. (5), is rewritten as

$$\mathbf{p} = k\mathbf{w} \text{ or in components } \begin{cases} p_n = kw_n, \\ p_\tau = kw_\tau, \end{cases} \tag{7}$$

where the subscript n indicates the normal direction and the subscript τ indicates the tangential direction to the surface, and k is a function of a number of parameters as will be described in the following. Note that the above equation is for the opening mode where $w_n > 0$; the contact and friction mode where $w_n = 0$ will be discussed later.

The behavior for the cohesive zone material as shown schematically in the phase space (p, w) in Fig. 2b is proposed, within the framework of a line spring model. The phase space coordinates p and w are the magnitudes of the traction and displacement jump vectors, i.e., $p = |\mathbf{p}|$ and $w = |\mathbf{w}|$. Under monotonic loading, the cohesive zone material reaches a maximum traction, and then follows a locus with softening stiffness. This locus is termed as the damage locus, and the cohesive zone is limited to develop along this locus. The reduction of the stiffness is assumed to be irrecoverable, indicating an irreversible damage process in the cohesive zone. Under monotonic loading, the damage locus is given by

$$p_\mathrm{d} = \bar{p}_\mathrm{d}(w_\mathrm{d}), \tag{8}$$

where $w_\mathrm{d}(= w)$ is taken to be the damage parameter. Under cyclic loading, the cohesive zone may accumulate damage even when cycled below the damage locus; without losing generality, a polynomial expression for the cyclic behavior is postulated, as described for loading and unloading paths, respectively, in the following. For a loading path, $\dot{w} > 0$, the stiffness k is expressed as a function of w_d and w in a polynomial expansion:

$$k = \bar{k}_1(w, w_\mathrm{d}) = \begin{cases} (p_\mathrm{d}/w_\mathrm{d})\left(1 + \sum_{l=1}^{L} \alpha_l (w/w_\mathrm{d})^l\right) \Big/ \left(1 + \sum_{l=1}^{L} \alpha_l\right) & \text{if } w < w_\mathrm{d}, \\ p_\mathrm{d}/w & \text{if } w = w_\mathrm{d}, \end{cases} \tag{9}$$

where w_d is the irreversible damage parameter as defined above, and α_l and L are the fitting constants describing the loading behavior and may be dependent in general on w_d. To complete the description, the evolution law for w_d under $\dot{w} > 0$ is given by

$$\dot{w}_\mathrm{d} = \begin{cases} 0 & \text{if } w < w_\mathrm{d}, \\ \dot{w} & \text{if } w = w_\mathrm{d}. \end{cases} \tag{10}$$

Therefore, under monotonic loading, the damage parameter w_d is a constant until the material reaches the damage locus. Under continued loading, the material behaves following the damage locus, with w_d increasing at the same rate as w. Similarly, for an unloading path, $\dot{w} < 0$, the stiffness k is expressed, as a function of w and w_d, by

$$k = \bar{k}_2(w) = \left(p^{(\mathrm{turn})}/w^{(\mathrm{turn})}\right)\left(1 + \sum_{m=1}^{M} \beta_m (w/w_\mathrm{d})^m\right) \Big/ \left(1 + \sum_{m=1}^{M} \beta_m \left(w^{(\mathrm{turn})}/w_\mathrm{d}\right)^m\right), \tag{11}$$

where $p^{(\mathrm{turn})}$ and $w^{(\mathrm{turn})}$ are the traction and displacement jump at the point when the unloading begins, and β_m and M are the fitting constants describing the unloading behavior and may be dependent on w_d as well as $p^{(\mathrm{turn})}$ and $w^{(\mathrm{turn})}$. Note that in the above equation the damage parameter w_d may change during the unloading process, which may be determined based on the current state (p, w) using Eq. (9). It is normally required that $\dot{w}_\mathrm{d} \geqslant 0$ to hold for all time guaranteeing irreversibility of damage. This requires that

$$\sum_{l=1}^{L}\alpha_l(w/w_{\mathrm{d}})^l < 0 \quad \text{and} \quad \sum_{m=1}^{M}\beta_m(w/w_{\mathrm{d}})^m > 0. \tag{12}$$

Along the damage locus, there in general exist two critical parameters, p_y, the maximum traction at damage initiation, and w_f, the maximum displacement jump at complete breakage. A point at p_y corresponds to a tip of the cohesive zone, which is also called the fictitious crack tip. The first point at which $w_{\mathrm{d}} \leqslant w_f$ towards the cohesive zone tip is defined to be the physical crack tip. The points in between these two tips along a crack line is defined to be the cohesive zone or the fracture process zone. Note that at the physical crack tip, the opening displacement jump may not be equal to w_f, but the traction must be equal to zero indicating the complete debonding of the material.

It should be remarked that the physical meaning of the damage parameter w_{d} in this case is not as simple as the maximum displacement jump that the cohesive zone material has ever experienced as shown by Yang and Ravi-Chandar (1998b) and others. On the one hand, the material may undergo damage along the damage locus with increasing w_{d} set equal to this quantity (the current w) under monotonic loading, as indicated in Eq. (10). On the other hand, w_{d} may increase irreversibly as well during unloading. Therefore, unlike in all of the previous models (Ortiz, 1996; Yang and Ravi-Chandar, 1996, 1998a,b; de-Andres et al., 1999), it is intrinsically modeled in the present formulation that the material may accumulate damage upon unloading even when it is below the damage locus. With this formulation, subcritical fatigue crack growth due to cyclic loading within the cohesive zone can be modeled. The rate of fatigue crack growth is determined by the fitting coefficients that quantify the severity of the nonlinearity under cyclic loading.

In order to characterize the law described above experimentally, we suppose that the cohesive zone material at the current w_{d} is loaded from the origin to a displacement jump $w_{\mathrm{c}}(< w_{\mathrm{d}})$, and then unloaded back to the origin. Note that $w_i^{(0)} = 0$ is assumed. The reduction in the stiffness k due to this cycle may be derived from the above equations, as

$$d\ln k/\mathrm{d}N = \left(\sum_{l=1}^{L}\alpha_l(w_{\mathrm{c}}/w_{\mathrm{d}})^l - \sum_{m=1}^{M}\beta_m(w_{\mathrm{c}}/w_{\mathrm{d}})^m\right) \Bigg/ \left(1 + \sum_{m=1}^{M}\beta_m(w_{\mathrm{c}}/w_{\mathrm{d}})^m\right), \tag{13}$$

where N represents the number of cycles, and ln represents the natural logarithm. In the derivation of the above expression, it is assumed that the changes in w_{d} and k are very small in one cycle. Note that, for cases with very small $\sum_{m=1}^{M}\beta_m(w_{\mathrm{c}}/w_{\mathrm{d}})^m$, the rate of change of $\ln k$ is scaled nearly linearly with the coefficients. It means that the fatigue crack growth within the present model may be simulated in a reduced time scale by scaling; this is obviously meaningful when studying high-cycle fatigue. The above equation also suggests a way to determine the coefficients in experiments. For example, in the post fracture tensile (PFT) test of a fracture process zone (Hay and White, 1997), the cyclic behavior of a material element under load or displacement control may be easily achieved. By knowing the damage locus (hence $w_{\mathrm{c}}/w_{\mathrm{d}}$) and the stiffness reduction rates at different load levels, the coefficients α_l and β_m may be determined over the entire spectrum of w_{d}. This may also be achieved by in situ local measurement of the traction-crack displacement jump curve in the fracture process zone in a cyclic test at load ratio $R = 0$. The details of the experimental aspects in the determination of these coefficients will be discussed elsewhere.

Under arbitrary loading, the cracks may be in partial or complete contact. This problem is important in many engineering applications, particularly in fatigue failures. The effects of crack contact and possible friction must be incorporated into the present formulation in order to simulate the fatigue crack growth under arbitrary loading. When the crack contact occurs, Eq. (6), i.e., $w_n = 0$, is enforced. The frictional force is modeled through a Coulomb-type law. Thus, the tangential interaction of the crack surfaces in contact is given by

$$p_\tau = p_\tau^{\mathrm{cz}} - \mathrm{sign}(\dot{w}_\tau) f p_n, \tag{14}$$

where the first term p_{τ}^{cz} is the contribution due to the cohesive zone material in shear if it is not completely broken, and the second term represents the Coulomb friction component in which f denotes the coefficient of friction. Note that this contact and friction description is a very simple one based on the assumptions of small relative sliding and simple geometry of the contact crack surfaces. Nevertheless, it completes the formulation of the cohesive zone model for fatigue crack growth under arbitrary loading condition. Under continuous loading, the cracks may grow naturally due to the finite strength and toughness of a material, and a criterion for crack advance needs to be furnished. With this criterion addressed next, the formulation of the fatigue crack growth in quasibrittle materials will be completed.

2.3. The maximum principal stress criterion for crack growth

Two properties, the strength and the dissipation capacity of a material around a crack tip, are fundamental to crack propagation analysis. When stresses at a crack tip reach the strength, a crack starts to develop a fracture process zone around the tip, but without crack propagation. After the process zone is fully developed, or nominally fully developed in a case of structural instability or in a case of fatigue, the crack tip starts to move as well with the process zone tip. Several criteria for crack advance in brittle materials have been proposed associated with the singularity-based stress analyses, which take care of the dissipation capacity (Qian and Fatemi, 1996). In the cohesive zone model of quasibrittle materials, the material strength is primarily considered in advancing the cohesive zone tip while the dissipation capacity is implicitly modeled in the cohesive force law with the cohesive zone thickness as the intrinsic physical length scale. Therefore, while the crack growth modeled in the cohesive zone model is critical in strength, it may be subcritical in toughness with energy dissipation below the maximum possible value for all circumstances. From this point of view, the cohesive zone model is more flexible and powerful than the singularity-based fracture mechanics approaches as long as the basic assumptions on the zone dimensions are satisfied.

In the following simulations of the fatigue crack growth, a criterion based on the maximum principal stress at the cohesive zone tip is used. This criterion states that the cohesive zone tip is ready to advance when the maximum principal stress reaches a critical value in the direction normal to the maximum principal stress. This maximum principal stress criterion (MPS criterion) is established based only on the material strength and is set up merely as a tensile stress limit. In some cases, the shear stress at a crack tip may be very high, indeed exceeding the shear strength of a material. For instance, in fretting fatigue tests, it has often been observed that a short crack first initiates at the edge of contact along the direction of maximum shear stress, and it then kinks to a mode I dominant path after a certain depth (Endo and Goto, 1976; Nix and Lindley, 1985). Hence a limit needs to be set up as well for induction of the bulk material into the cohesive zone in the shear mode; this is consequently called the maximum shear stress (MSS) criterion. These two criteria form a locus in the stress space for propagation of the cohesive zone tip. In the following simulations, however, only the MPS criterion is used for simplicity. For the numerical marching aspects applying this law, one may refer to Yang (1998). Now, we turn to the numerical simulations of fatigue crack growth, solved using the iterative single-domain dual-boundary-element method for cohesive cracks in elastostatics (Yang and Ravi-Chandar, 1998b).

3. Fatigue crack growth simulations and discussions

Given the constitutive properties of the cohesive zone, subcritical crack growth may be predicted for arbitrary cyclic loading conditions. A number of issues regarding accumulation of fatigue damage and crack growth may be investigated. In the following study, we assume a particular form for the stiffness k of the cohesive zone. With only $\alpha_1 \neq 0$ and with all $\beta_m = 0$, a quadratic loading path and a linear unloading path is considered, independent of w_d. The nonzero constant α_1 controlling the severity of nonlinearity

governs the rate of the fatigue damage and crack growth, as indicated in Eq. (13). Note that the initial w_d (and hence initial k) representing a physical initial flaw plays a role on the fatigue life, also as indicated in Eq. (13). Furthermore, the damage locus is assumed to be a straight line, simply characterized by the parameters p_y and w_f; correspondingly, the critical J-value for static crack growth is $J_{sc} = p_y w_f/2$, and the critical elastic stress intensity factor for stable crack growth in mode I under static loading is $K_{sc} = \sqrt{E p_y w_f/2}$. Therefore, given the values of α_1, p_y, w_f and initial w_d, the fatigue behavior of the cohesive zone is completely determined. In Section 3.1, mode I crack initiation and growth are examined using a single-edge-notched tension (SENT) specimen. In Section 3.2, mixed-mode fatigue crack growth under nonproportional loading is examined. In these simulations, a system with a maximum of 240 nodes (80 quadratic discontinuous elements) was used, resulting in a system of 480 equations plus the constitutive equations for the cohesive zone nodes. The code (Yang and Ravi-Chandar, 1998b) was run on a Digital Personal Workstation 433 au. It took about 2 CPU seconds to complete one loading step of the computation; the convergence of the iterative process was checked to ensure the reliability of the solution. With this computer speed and the efficiency of the code, a computational fatigue test under the number of loading cycles up to 10^5 becomes feasible. We chose a relatively large $\alpha_1 (= 0.1)$ with which the fatigue life of the specimen is limited to about a few thousands cycles so as to finish each of the computational tests in a couple of CPU hours.

3.1. Mode I fatigue crack growth

It is first examined the mode I fatigue crack growth simulated in the SENT specimen, as shown in Fig. 3 with loading angle $\theta = 90^\circ$ with aspect ratio $h/l = 1$. The specimen length, l, is taken to be the characteristic length scale. Note that, in the event of fracture, it might be more appropriate to consider the length scale in the fracture process zone (the cohesive zone), such as the thickness of the cohesive zone, as the characteristic length scale. However, it appears more convenient to use the specimen size l since most of the

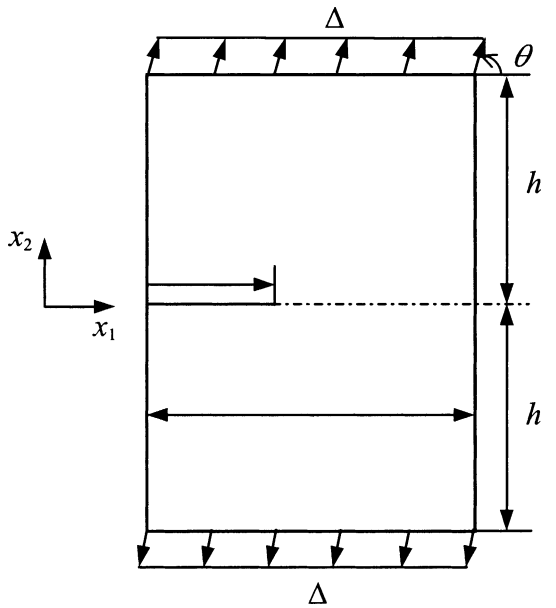

Fig. 3. A sketch of the specimen: Two cases of $\theta = 0$ and 90°, respectively are used in the present study. The aspect ratio $h/l = 1$. The second case of symmetry is called the SENT specimen in convention.

following discussions are made on the global scale. The shear modulus, μ, is taken to scale traction and stress quantities. In the simulation, the boundaries are discretized into three (quadratic discontinuous) elements per l. The initial crack is of length $0.2l$ and is discretized into five elements with their sizes decreasing by a grading factor of 0.85 from the specimen edge to the interior. A tiny initial damage zone is assumed at the crack tip. The crack is extended straight ahead in pure mode I due to symmetries of the configuration and load in a step size of $0.01l$; at each step of advance, a new crack element is created of the same size. The time variation of displacement magnitude at the loading boundaries is given in Fig. 4. The initially stress-free specimen is loaded to a maximum displacement $\Delta_{\max}$, subsequently unloaded to a minimum displacement $\Delta_{\min}$, and then subjected to the cyclic displacement between $\Delta_{\max}$ and $\Delta_{\min}$; these quantities are taken to be $\Delta_{\max} = 9E-4l$ and $\Delta_{\min} = 5E-4l$ in the numerical simulations. As rate-dependence of the cohesive zone behavior is ignored in the constitutive description, the frequency and shape of the load variation do not affect the fatigue life. The load increment during loading is $1E-4l$, while the unloading from $\Delta_{\max}$ to $\Delta_{\min}$ is completed in one step because of the linearity of the unloading process. Sensitivity of the computation to load increment during loading was tested; the results using a one-step load from $\Delta_{\min}$ to $\Delta_{\max}$ are no different from those using the incremental procedure by a step of $1E-4l$. The material parameters are: $\alpha_1 = 0.1$, $p_y = 0.01\mu$, and $w_f = 0.001l$; correspondingly, $J_{sc} = 5E-6\mu l$ and $K_{sc} = 3.6E-3\mu l^{1/2}$. The initial w_d is taken to be $1.0E-9l$. The results of the simulation are presented in Figs. 5–8. In Fig. 5, the evolution of the fictitious and physical crack tips with the number of loading cycles and the crack growth rate versus crack tip position are shown. Two typical crack opening profiles and the corresponding traction profiles before and after movement of the physical crack tip are shown in Fig. 6. By correlating the traction and the crack opening displacement, the J-integral for crack advance can be evaluated. The J-integral may further be converted into the effective stress intensity factor K_I by $K_I = \sqrt{EJ}$ for the pure mode I crack. The maximum and the minimum of the stress intensity factor, normalized by K_{sc}, i.e., $\widetilde{K}_{\max}$ and $\widetilde{K}_{\min}$, corresponding to $\Delta_{\max}$ and $\Delta_{\min}$, respectively, are plotted against the physical crack tip position in Fig. 7, and compared with the linear elastic fracture mechanics (LEFM) solutions. The history of a typical cohesive zone node at $x_1/l = 0.4$ is plotted in terms of traction and displacement jump in Fig. 8. Some discussions of these results are described in the following:

- In the first loading path, the fictitious crack tip extends a couple of increments while the physical crack tip is stationary, as shown in Fig. 5a. If the load is held at the first peak, which is below the critical load for the full-size cohesive zone, the fictitious crack tip should stop with no further damage accumulation or cracking of the material. However, under the subsequent cyclic loading, the cohesive zone material

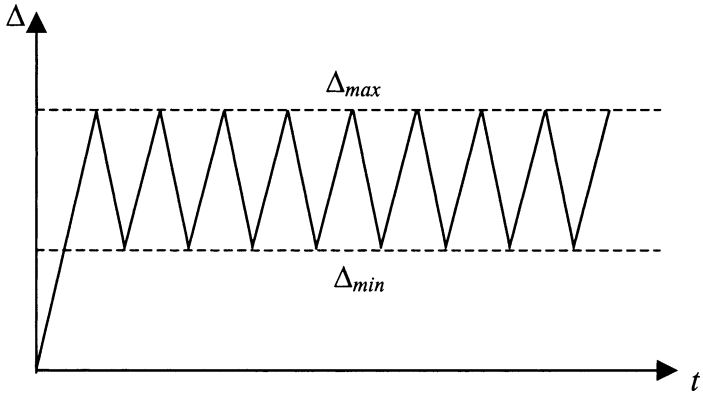

Fig. 4. Variation of the displacement magnitude Δ at the loading boundaries with time. The frequency and shape of the load variation do not affect the fatigue behavior because the rate-dependence of the material is ignored.

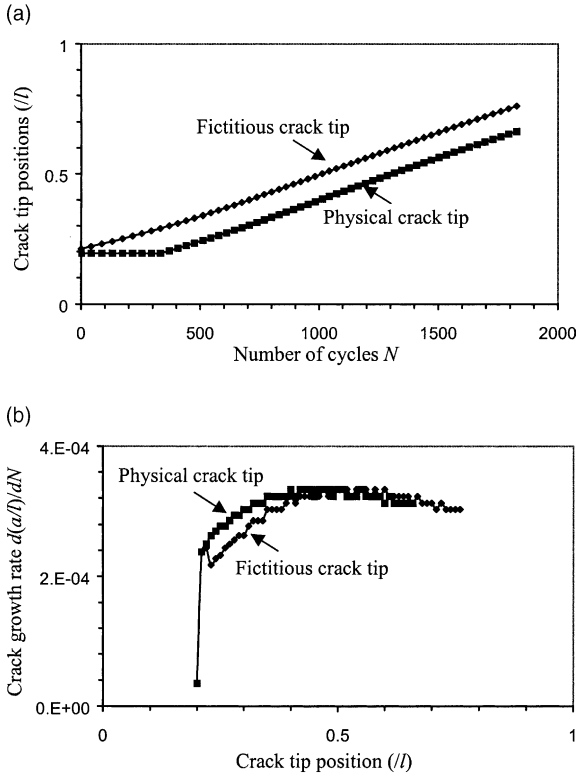

Fig. 5. Evolution of the physical and fictitious crack tips: (a) crack tip position versus number of loading cycle and (b) crack growth rate versus tip position.

undergoes continuous damage with a softening stiffness, as shown in Fig. 8. The gradual loss of load carrying capacity in the trailing process zone enhances the stress state at the fictitious crack tip and drives it to extend further.

- The physical crack tip starts to move with the fictitious crack tip after the cohesive zone of size $0.09l$ is developed. This cohesive zone size is maintained in the subsequent steady-state crack growth, which is a little smaller than the full size of $0.1l$ observed in the static-loading simulation with the same material properties (Yang and Ravi-Chandar, 1998b).
- The rate of the crack growth varies as the crack extends, in correspondence to the variation of the driving force, as shown in Figs. 5b and 7. Note that the maximum K_{I} for crack advance at the cyclic loading condition is about 30% below the static toughness K_{sc}, indicating a subcritical crack growth. Therefore, the subcritical crack growth due to cyclic loading has successfully been modeled in the present cohesive zone model by taking account of the difference of loading and unloading paths of the cohesive zone material.
- It should be noted that, as shown in Fig. 8, the nonlinearity in the cohesive zone, which leads to a fatigue life of a few thousands of cycles, appears to be very small. This suggests that the constants α_l (α_1 only, in this case) may not be a quantity that is directly measurable from static-loading experiments. Calibration from fatigue tests for these constants (applying for example Eq. (13)) is necessary.

This simulation illustrates that with the given material properties, fatigue crack initiation (from a pre-crack, in contrast to crack nucleation from a flaw) and growth can be modeled in a unified manner using a

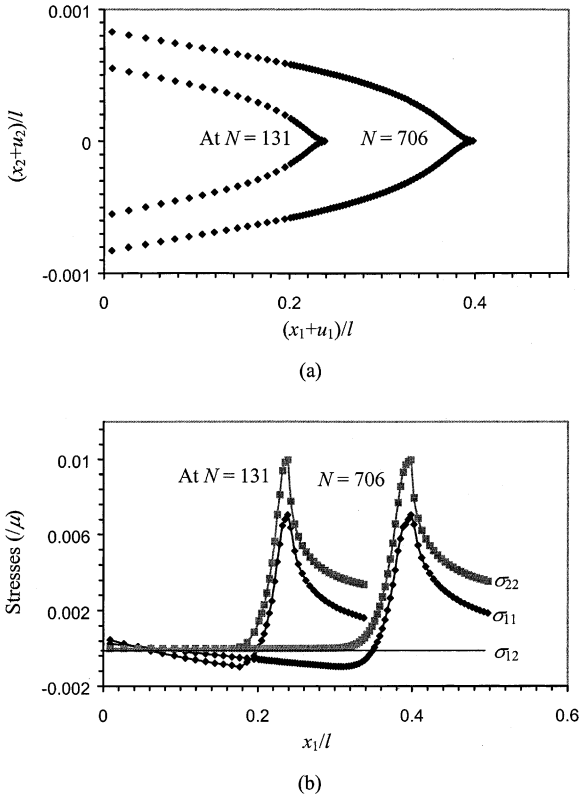

Fig. 6. (a) Crack opening profiles at $\Delta = \Delta_{\max}$ at $N = 131$ and 706, respectively and (b) the corresponding stress components along the crack line. At $N = 131$, the cohesive zone is under development with only the fictitious crack tip advanced. At $N = 706$, the crack grows in steady state with the cohesive zone size of $0.09l$. Note that the stress component σ_{22} is equal to $p_y(= 0.01\mu)$ indicating the critical state at the fictitious crack tip with respect to material strength. Meanwhile, the energy release rate is less than the material toughness under static loading.

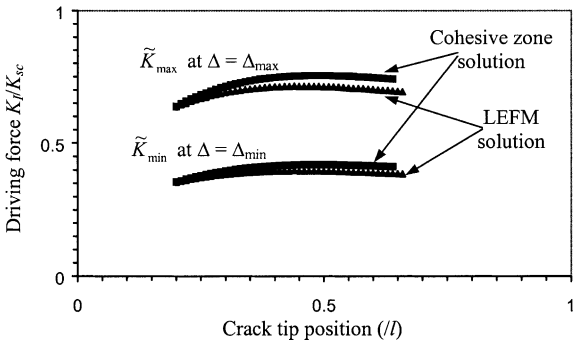

Fig. 7. Range of the effective stress intensity factor converted from the J-integral evaluated during the fatigue crack growth, compared to the driving forces predicted by LEFM. Note that the maximum K_I is about 30% below the material toughness K_{sc} at static loading indicating a subcritical crack growth process.

cohesive zone model. The number of cycles required for fatigue crack initiation as well as the growth rate of a fatigue crack is uniquely determined by loading conditions and material properties. In the following, we

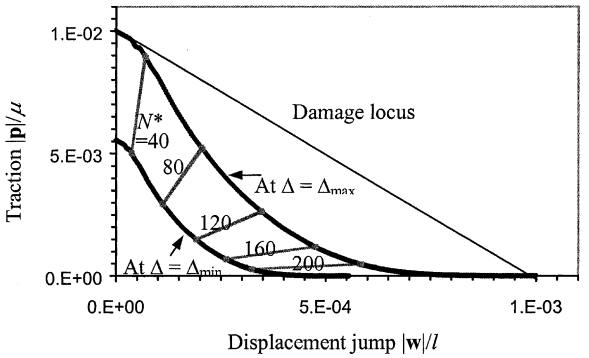

Fig. 8. History of a typical cohesive zone node at $x_1/l = 0.4$, indicating continuous accumulation of damage and softening spring stiffness with number of loading cycles. The limits at $\Delta = \Delta_{\max}$ and $\Delta_{\min}$ are drawn, as well as a few pairs of successive paths between the limits at the numbers of cycles beyond the initiation of damage, N^*, as indicated. Note that the damage process is well below the damage locus.

show a relationship between the growth rate and the loading conditions for the model material with only $\alpha_1 \neq 0$.

A number of simulations were run for various $\Delta_{\max}$ and $\Delta_{\min}$, with all other features kept the same as in the previous simulation. The crack growth rate $\mathrm{d}a/\mathrm{d}N$ of the physical crack tip at $x_l/l = 0.45$ (for a fixed $\widetilde{K}_{\max}$) in each of the simulations is calculated; the results are plotted in Fig. 9. First, it is seen that the crack growth rate is nearly linearly dependent on $(\widetilde{K}_{\max} - \widetilde{K}_{\min})$ for example with $\widetilde{K}_{\max}$ fixed at 0.707 and 0.471, respectively. It is suggested that this linear relationship would be valid for all $\widetilde{K}_{\max}$, i.e.,

$$\frac{\mathrm{d}(a/l)}{\mathrm{d}N} = A\left(\widetilde{K}_{\max}\right)\Delta\widetilde{K}, \tag{15}$$

where $\Delta\widetilde{K} = \widetilde{K}_{\max} - \widetilde{K}_{\min}$, and A is a function depending on $\widetilde{K}_{\max}$. Thus, it suffices that the function A of $\widetilde{K}_{\max}$ is determined in order for all range of the fatigue behavior. The crack growth rates at various $\widetilde{K}_{\max}$ and $\widetilde{K}_{\min} = 0$ obtained from these simulations are shown in Fig. 9; the function A is then determined for different $\widetilde{K}_{\max}$ as given in Fig. 10, showing a strong dependence of the coefficient constant on the maximum load (or equivalently the mean load). The form in Eq. (15) is a special case of Paris's law for fatigue crack growth. The behavior of the fatigue crack described above is obviously a consequence of the cohesive force law assumed (with only $\alpha_1 \neq 0$). For real materials, the polynomial expression in Eq. (9), which fits a nonlinear loading path, may consist of more than one term, resulting in a more complicated behavior than what we have seen here. However, the concepts in the present cohesive zone model of fatigue crack growth

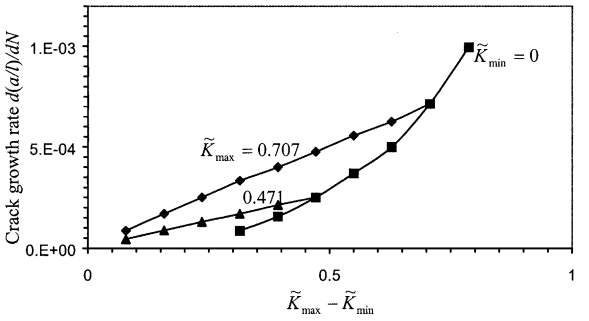

Fig. 9. Variation of the fatigue crack growth rate with magnitude and range of the effective stress intensity factor.

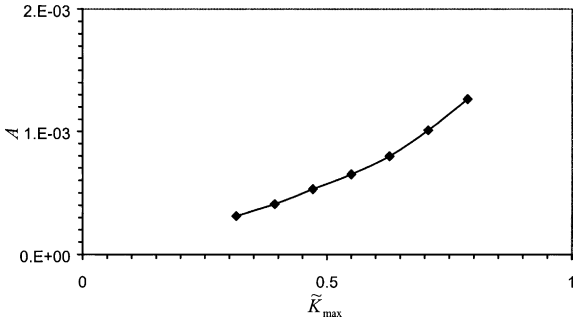

Fig. 10. Variation of the coefficient A in Eq. (15) with K_{max}, indicating the strong dependence of crack growth rate with magnitude (or equivalently mean value) of the load.

based on known local material properties developed in the present work can be carried over to more complex cohesive force laws. Using the present model, it is easy to investigate issues, such as fatigue crack growth under nonproportional and even random cyclic loads encountered frequently in engineering problems. In the following, fatigue crack growth under mixed-mode loading is simulated.

3.2. Fatigue crack growth under mixed-mode loading

In the above examples, we have demonstrated many features of fatigue crack initiation and growth using a cohesive zone model, and hence predictability of fatigue under mode I loading. Given an appropriate criterion for crack advance, this model can also simulate fatigue crack growth under more complicated loading conditions. In order to demonstrate this, we work again with the specimen shown in Fig. 3, but this time with a loading angle $\theta = 0^\circ$. Consequently, a shear load is applied to the specimen, and the crack is subjected to a pure mode II loading. The crack should kink upon initiation of crack growth and then follow a curved, smooth path according to the MPS criterion as described in Section 2. Results from one such simulation are presented in Figs. 11–14. In this simulation, the coefficient of friction f is taken to be zero, and the maximum load-point displacement $\Delta_{max} = 3E - 3l$ and the minimum load-point displacement $\Delta_{min} = 3E - 3l$. All the other material properties and computational features are the same as in the previous simulations. The predicted crack path is shown in Fig. 11, and compared with the LEFM prediction using the maximum tangential stress (MTS) criterion (Erdogan and Sih, 1963). The growth rate of the physical crack tip along the path is calculated and plotted against position in Fig. 12. The J-integral (equivalently, the effective stress intensity factor K_I) at the moment of crack growth along the path is calculated and plotted in Fig. 13, compared with the corresponding LEFM solution at $\Delta = \Delta_{min}$. The history of a typical cohesive zone node at crack arc length $a/l = 0.4$ is shown in terms of traction and displacement jump in Fig. 14. The results of this simulation indicate a number of features about fatigue crack growth:

- First, it is seen in Fig. 11 that the crack path predicted using the MPS criterion in the cohesive zone model is nearly the same as predicted using the MTS criterion in the LEFM approach. The crack was initiated and grown by the largest maximum principal stress at the crack tip achieved at $\Delta = \Delta_{min}$, which is consistent to the LEFM solution which was obtained at a constant $\Delta = \Delta_{min}$.
- Beyond initiation, the crack growth rate increases nearly linearly, as shown in Fig. 12. The increase of growth rate corresponds to an increase of driving force along with the crack extension, as shown in Fig. 13. Again, the effective stress intensity factor evaluated during the fatigue crack growth is consistent with the prediction using the simpler LEFM approach. However, in this case, the local loading condition on a crack tip can no longer be characterized simply by two parameters as in the previous case of a mode I

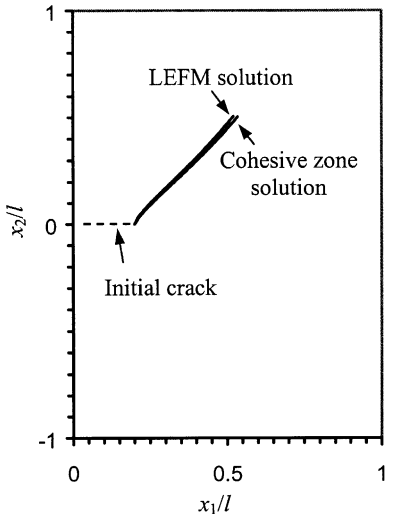

Fig. 11. Crack path predicted under the action of the tangential alternating load on the top and bottom boundaries. The predictions using the MPS criterion in the cohesive zone model and using the MTS criterion in the LEFM approach are close, since both the criteria predict a mode I crack growth.

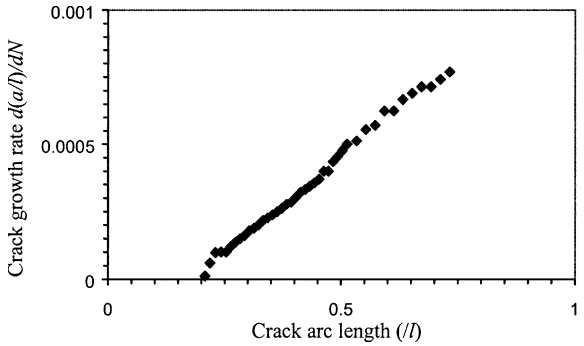

Fig. 12. Variation of the fatigue crack growth rate with crack arc length along the curved path shown in Fig. 11.

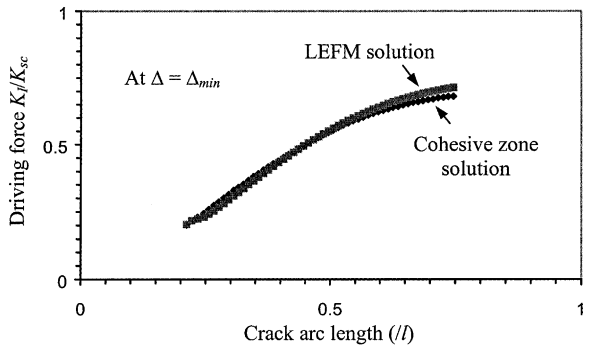

Fig. 13. Variation of the maximum energy release rate (in form of equivalent K_I) with crack arch length along the curved path shown in Fig. 11, compared to the LEFM prediction. Note that the crack growth occurred at $\Delta = \Delta_{\min}$.

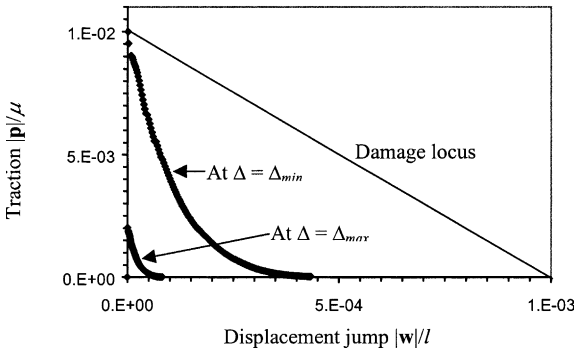

Fig. 14. History of a typical cohesive zone node at crack arc length $a/l = 0.4$, under the mixed-mode cyclic loading. Only the states at $\Delta = \Delta_{\min}$, 0 and $\Delta_{\max}$ are shown by symbols. During one cycle, this point behaves from the origin to the upper limit, back to the origin, up to the lower limit, back to the origin and so forth. However, the stiffness kept decreasing with number of loading cycles during the cyclic process.

crack. The driving force for crack advance changes its magnitude as well as its orientation continuously during the cyclic loading, as will be shown below. A simple description of fatigue in such a case in terms of magnitude of K and range of K ignoring details in the fracture process zone is obviously insufficient.

- A better view of the fatigue damage process under nonproportional loading is obtained by examining the evolution of damage at a typical cohesive zone node, as shown in Fig. 14. The states of the cohesive zone node at $\Delta = \Delta_{\min}$, 0, and $\Delta_{\max}$, respectively are indicated by symbols; note that $\Delta_{\min}$ is negative and $\Delta_{\max}$ is positive in the simulation. During one cycle, this point experiences two extremes of load at $\Delta = \Delta_{\min}$ and $\Delta_{\max}$. During the loading from $\Delta = 0$ to $\Delta_{\min}$ and back to 0, the crack is open; the traction p evolves correspondingly from 0 to the higher of the two peaks and back to 0. During the load from $\Delta = 0$ to $\Delta_{\max}$ and back to 0, the crack is closed and deforms in shear mode only; the traction p in this time evolves between 0 and the lower of the two peaks. Thus, the cohesive spring is subjected to a complicated local bimodal cyclic loading. In this simulation, it has been ignored friction effects along the crack surfaces. The role of friction in this case is simple to hold somehow the relative sliding between the crack surfaces when the crack is in contact. The presence of friction may decelerate the fatigue crack growth.

It should be remarked that the present cohesive zone model has provided a more general strategy to model fatigue crack problems in quasibrittle materials. Once the local material property around a crack tip is known, the fatigue crack initiation and growth may be simulated in a unified way and be predicted for arbitrary loading conditions. To solve a problem of an asymmetric crack under nonproportional local load, the cohesive zone model, taking account of the details of the material behavior in the fracture process zone, is obviously more advantageous and flexible than the LEFM and other singularity-based fracture mechanics approaches. Furthermore, the incorporation of local material behavior in a crack model is important in modifying and redesigning materials.

4. Conclusions

We have proposed a general strategy to model the fatigue damage and crack growth in quasibrittle materials using the cohesive zone model. While the bulk material is modeled to be linearly elastic, the softening material in the cohesive zone and the cracks are modeled to be singular surfaces in the elastic body. In all the previous cohesive zone models in the literature, the cohesive zone material was either re-

stricted to the damage locus or assumed to behave linearly under loading, unloading and reloading below the damage locus. In the former case, the model is justified only for cracks under monotonic loading conditions. In the latter, although it is supposed to be capable of simulating crack growth under arbitrary loading conditions, the model is yet incapable of predicting subcritical fatigue crack growth due to cyclic loading. In the present model, the characteristic behavior of the cohesive material responsible for the fatigue damage, and crack growth is modeled by creating a difference between the loading and unloading paths and is built in a general polynomial form. Subcritical fatigue crack initiation as well as growth is then predicted in a unified way, without imposing explicit rules for the initiation life and growth rate as in the classical singularity-based fracture mechanics approaches. The maximum principal stress criterion is used to advance a tip of the cohesive zone; fatigue crack growth occurs as a natural process of debonding of the cohesive material under cyclic loading. The iterative single-domain dual-boundary-element method of successive over-relaxation introduced by Yang and Ravi-Chandar (1998b) is extended to solve the formulated boundary-value problem, which is nonlinear due to the nonlinearity and history dependence of the cohesive zone material. Within the formulation, the fatigue crack growth in a single-edge-notched rectangular specimen in pure mode I and in mixed-mode is simulated and discussed in detail, demonstrating the capability of the present model to predict fatigue crack initiation and growth in quasibrittle materials.

Acknowledgements

The authors gratefully acknowledged the support of U.S. Air Force Office of Scientific Research.

References

Barenblatt, G.I., 1962. The mathematical theory of equilibrium cracks in brittle fracture. In: Dryden, H.L., von Karman, T. (Eds.), Advances in Applied Mechanics, vol. VII. Academic Press, New York, pp. 55–129.

Bazant, Z.P., Ozbolt, J., Eligehausen, R., 1994. Fracture size effect: review of evidence for concrete structures. ASCE Journal of Structural Engineering 120, 2377–2398.

Bazant, Z.P., Li, Y.-N., 1995. Stability of cohesive crack model: Part I – Energy principles. Transactions of ASME, Journal of Applied Mechanics 62, 959–964.

Bazant, Z.P., Li, Y.-N., 1997. Cohesive crack model with rate-dependent opening and viscoelasticity: I. Mathematical model and scaling. International Journal of Fracture 86, 247–265.

Begley, M.R., Cox, B.N., McMeeking, R.M., 1997. Creep crack growth with small scale bridging in ceramic matrix composites. Acta Materialia 45, 2655–3088.

Carpinteri, A., 1994. Cracking of strain-softening materials. In: Aliabadi, M.H., Brebbia, C.A., Parton, V.Z. (Eds.), Static and Dynamic Fracture Mechanics. Computational Mechanics, Southampton, pp. 311–365.

de-Andres, A., Perez, J.L., Ortiz, M., 1999. Elastoplastic finite element analysis of three-dimensional fatigue crack growth in aluminum shafts subjected to axial loading. International Journal of Solids and Structures 36, 2175–2320.

Dugdale, D.S., 1960. Yielding in steel sheets containing slits. Journal of the Mechanics and Physics of Solids 8, 100–104.

Endo, K., Goto, H., 1976. Initiation and propagation of fretting fatigue cracks. Wear 38, 311–324.

Erdogan, F., Sih, G.C., 1963. On the crack extension in plates under plane loading and transverse shear. Journal of Basic Engineering, ASME Transactions 91, 764–769.

Hay, J.C., White, K.W., 1997. The stiffness of grain bridging elements in a monotonic alumina. Journal of American Ceramic Society 80, 1293–1297.

Hillerberg, A., Modeer, M., Petersson, P.E., 1976. Analysis of crack formation and crack growth in concrete by means of fracture mechanics and finite elements. Cement and Concrete Research 6, 773–782.

Li, Y.N., Hong, A.P., Binienda, W.K., 1998. Theory of cohesive crack model with interactive cracks. International Journal of Solids and Structures 35, 981–994.

Nix, K.J., Lindley, T.C., 1985. The application of fracture mechanics to fretting fatigue. Fatigue and Fracture of Engineering Materials and Structures 8, 143–160.

Ortiz, M., 1996. Computational micromechanics. Computational Mechanics 18, 321–338.

Qian, J., Fatemi, A., 1996. Mixed mode fatigue crack growth: a literature survey. Engineering Fracture Mechanics 55, 969–990.
Williams, M.L., 1957. On the stress distribution at the base of a stationary crack. Journal of Applied Mechanics 24, 109–114.
Xu, X.-P., Needleman, A., 1994. Numerical simulations of fast crack growth in brittle solids. Journal of the Mechanics and Physics of Solids 42, 1397–1434.
Yang, B., 1998. A boundary element methodology for crack path prediction in brittle materials incorporating a cohesive zone model. Ph. D. Thesis, University of Houston.
Yang, B., Ravi-Chandar, K., 1996. On the role of the process zone in dynamic fracture. Journal of the Mechanics and Physics of Solids 44, 1955–1976.
Yang, B., Ravi-Chandar, K., 1998a. Antiplane crack growth under quasistatic loading in a damaging material. International Journal of Solids and Structures 35, 3695–3715.
Yang, B., Ravi-Chandar, K., 1998b. A single-domain dual-boundary-element formulation incorporating a cohesive zone model for elastostatic cracks. International Journal of Fracture 93, 115–144.